

Simulations of Baryon Acoustic Oscillations I: Growth of Large-Scale Density Fluctuations

Ryuichi Takahashi¹, Naoki Yoshida^{1,2}, Takahiko Matsubara¹, Naoshi Sugiyama^{1,2},
Issha Kayo², Takahiro Nishimichi³, Akihito Shirata^{3,4}, Atsushi Taruya^{3,5},
Shun Saito³, Kazuhiro Yahata³, and Yasushi Suto³

¹ *Department of Physics and Astrophysics, Nagoya University, Chikusa, Nagoya 464-8602, Japan*

² *Institute for Physics and Mathematics of the Universe, University of Tokyo, 5-1-5 Kashiwa-no-ha, Kashiwa City, Chiba 277-8582, Japan*

³ *Department of Physics, School of Science, The University of Tokyo, Tokyo 113-0033, Japan*

⁴ *Department of Physics, Tokyo Institute of Technology, Tokyo 152-8511, Japan*

⁵ *Research Center for the Early Universe, The University of Tokyo, Tokyo 133-0033, Japan*

ABSTRACT

We critically examine how well the evolution of large-scale density perturbations is followed in cosmological N -body simulations. We first run a large volume simulation and perform a mode-by-mode analysis in three-dimensional Fourier space. We show that the growth of large-scale fluctuations significantly deviates from linear theory predictions. The deviations are caused by *nonlinear* coupling with a small number of modes at largest scales owing to finiteness of the simulation volume. We then develop an analytic model based on second-order perturbation theory to quantify the effect. Our model accurately reproduces the simulation results. For a single realization, the second-order effect appears typically as “zig-zag” patterns around the linear-theory prediction, which imprints artificial “oscillations” that lie on the real baryon-acoustic oscillations. Although an ensemble average of a number of realizations approaches the linear theory prediction, the dispersions of the realizations remain large even for a large simulation volume of several hundred megaparsecs on a side. For the standard Λ CDM model, the deviations from linear growth rate are as large as 10 percent for a simulation volume with $L = 500h^{-1}\text{Mpc}$ and for a bin width in wavenumber of $\Delta k = 0.005h\text{Mpc}^{-1}$, which are comparable to the intrinsic variance of Gaussian random realizations. We find that the dispersions scales as $\propto L^{-3/2}\Delta k^{-1/2}$ and that the mean dispersion amplitude can be made smaller than a percent only if we use a very large volume of $L > 2h^{-1}\text{Gpc}$. The finite box size effect needs to be appropriately taken into account when interpreting results from large-scale structure simulations for future dark energy surveys using baryon acoustic oscillations.

Key words: cosmology:theory – large-scale structure of Universe – methods:N-body simulations

1 INTRODUCTION

Understanding the nature of dark energy that dominates the energy content of the universe is one of the main challenges in cosmology. The time evolution of the mysterious dark component is accessible only by astronomical observations. Baryon acoustic oscillations (BAO) can be used as a standard ruler by which precise measurement of the cosmological distance scale is achievable (e.g., Eisenstein, Hu & Tegmark 1998; Seo & Eisenstein 2003; Matsubara 2004).

Recent large galaxy redshift surveys, the Sloan Digital Sky Survey and the 2-degree Field survey, detected

the signature of the baryon acoustic peaks and thus provide constraints on the dark energy (Eisenstein et al. 2005; Cole et al. 2005; Percival et al. 2007; Okumura et al. 2007). Future observational programs will utilize the distribution of millions of high-redshift galaxies to detect BAO with higher accuracy. In order to properly interpret these observations, it is necessary to make accurate theoretical predictions for the length scale and other characteristic features of BAO (e.g. Nishimichi et al. 2007; Smith, Scoccimarro & Sheth 2008). Theoretically, a crucial issue is the non-linear evolution of matter and galaxy distributions (e.g., Seo & Eisenstein 2005; Angulo et al. 2007; Guzik, Bernstein & Smith 2007;

Smith, Scoccimarro & Sheth 2007). One usually resorts to using cosmological N -body simulations for this, but various effects –both physical and numerical– need to be understood in order to extract useful information. First of all, the power spectrum for a realization of a Gaussian random field has intrinsic deviations from expected values at any wavenumber, i.e., the mode amplitudes are Rayleigh-distributed (see e.g., Matsubara 2007a). A realization may thus show an additional oscillatory feature on large scales which compromises the true BAO signature (Huff et al. 2007). There are also a number of numerical issues. Accurate time integration is necessary in order to follow the evolution of large-scale density perturbations which have small amplitudes. Finite-box size limits the sampling of wavenumbers at the largest scales, where the power amplitude is dominated by only a few modes (Bagla & Prasad 2006 studied the finite box size effect on the mass function of dark matter halos.)

In this paper, we examine how accurately the evolution of large-scale density perturbations is followed in standard cosmological N -body simulations. In particular, we study the characteristic “wiggle” features which are often found in the matter power spectra calculated from N -body simulations in previous studies. We use an approach based on perturbation theory to study nonlinear effects in detail. A further extensive study is presented in a separate paper by Nishimichi et al. (in preparation).

Throughout the present paper, we adopt the standard Λ CDM model with matter density $\Omega_m = 0.241$, baryon density $\Omega_b = 0.041$, cosmological constant $\Omega_\Lambda = 0.759$, spectral index $n_s = 0.958$, amplitude of fluctuations $\sigma_8 = 0.76$, and expansion rate at the present time $H_0 = 73.2 \text{ km s}^{-1} \text{ Mpc}^{-1}$, consistent with the 3-year WMAP results (Spergel et al. 2007).

2 METHOD

2.1 The cosmological simulations

We use the cosmological simulation code Gadget-2 (Springel, Yoshida & White 2001; Springel 2005). For our fiducial runs, we employ 256^3 particles in a volume of $L = 500h^{-1} \text{ Mpc}$ on a side. We dump snapshots at a number of time steps (redshifts) to study the evolution of the density power spectrum. The simulation parameters are chosen such that sufficient convergence is achieved in the measured power spectrum at the present epoch (Takahashi et al., in preparation).

We generate initial conditions for our runs based on the standard Zel’dovich approximation using the matter transfer function calculated by CAMB (Code for Anisotropies in the Microwave Background; Lewis, Challinor & Lasenby 2000). The initial redshift is set to be $z_{\text{in}} = 30$. When we generate a realization for a Gaussian random field, the amplitude of each k -mode is assigned such that the ensemble follows the Rayleigh distribution. While the mean of the power is expected to approach the input value at k for an ensemble of large modes, the actual assigned power in a finite k -bin can deviate significantly from the expected value. Note also that a Rayleigh distribution has a positive skew, which causes the median to be smaller than the mean.

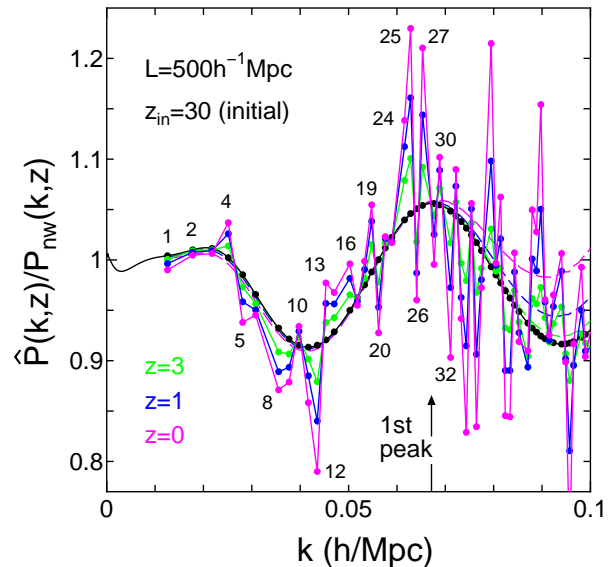


Figure 1. We plot the evolution of the power spectrum from the initial epoch (black line) to $z = 3$ (green), $z = 1$ (blue), and $z = 0$ (purple). The measured power spectrum is divided by the no-wiggle model of Eisenstein & Hu (1998). We subtract the intrinsic deviations from the input power spectrum at the initial epoch. The numbers indicate integer sums of $n_1^2 + n_2^2 + n_3^2$ of wavenumber vectors. The dashed lines are the one-loop power spectra at each redshift (see text).

2.2 Fourier mode analysis

We first compute the density field for each output of the N -body simulation. We use the CIC (cloud-in-cell) interpolation when assigning particles on grids. We check that the interpolation method does not affect the scales of interest ($k \lesssim 0.1$) by comparing various schemes. We then apply a Fast Fourier Transform¹ to obtain the density field $\delta(\mathbf{k})$ in three-dimensional Fourier space. We will examine both the amplitudes and the phases in detail in subsequent sections.

In order to study closely the Fourier mode-coupling, we calculate the mean amplitude of modes for a given realization with wavenumber vector $\mathbf{k} = (k_1, k_2, k_3)$ as

$$\hat{P}(k) = \frac{1}{N_k} \sum_{|\mathbf{k}|=k} |\delta(\mathbf{k})|^2, \quad (1)$$

where the summation is for all the wavenumbers of $|\mathbf{k}| = k = (k_1^2 + k_2^2 + k_3^2)^{1/2}$, N_k is the number of modes in k , and the wavenumber is discretized as $k_i = (2\pi/L)n_i$ with an integer n_i . An ensemble average of a number of realizations provides its expectation value of $P(k) = \langle \hat{P}(k) \rangle$.

In order to study the *evolution* of power spectrum, we divide the measured power spectrum in equation (1) at redshift z by the initial one at $z_{\text{in}} = 30$, and then multiply it by the input power spectrum. In this way, the initial random scatter included in the power spectrum is removed.

3 RESULTS

Fig.1 shows the evolution of power spectrum $\hat{P}(k)$ for a single realization. We show the mean amplitude for modes which have exactly the same wavevector norm, $|\mathbf{k}|^2 = k_1^2 + k_2^2 + k_3^2$, rather than binning in k . The vertical axis is the power spectrum divided by the no-wiggle model of Eisenstein & Hu (1999). The black line with symbols is the linear theory prediction with CAMB. The green, blue, and purple lines with dots are the measured mean values at each wave number at $z = 3, 1$, and 0 , respectively. The numbers in the figure indicate integer sums of $n_1^2 + n_2^2 + n_3^2$ of wavenumber vectors.

As clearly seen in the figure, the power amplitudes deviate from the linear theory prediction at low redshifts. The deviations appear to grow in time monotonically. Some modes (e.g. $n^2 = 4, 13, 19, 25, 27$) grow more rapidly than the linear growth, while other modes (e.g. $n^2 = 8, 12, 20, 26, 32$) grow less. These features can be seen even in higher resolution simulation of Springel et al. (2005) (see their Fig.6). Since the initial randomness of the amplitude of each mode has been already subtracted in the figure as described in section 2.2, the remaining differences plotted in Fig. 1 are due either to numerical integration errors or to some unknown physical effects. The deviations are indeed large, with the amplitudes being more than 10% at the scale of the first-peak of the BAO. It is thus important to understand and correct the apparent oscillatory features if these are artificial effects.

In the next section, we show that the deviations are *not* owing to numerical integration errors *but* due to the finite number of modes at the largest scales. We use second-order perturbation theory to explain the systematic deviations.

4 PERTURBATION THEORY

Second-order perturbation theory describes the evolution of a density perturbation as (e.g. Bernardeau et al. 2002)

$$\delta(\mathbf{k}, z) = \frac{D(z)}{D_{\text{in}}} \delta_1(\mathbf{k}) + \left(\frac{D(z)}{D_{\text{in}}} \right)^2 \delta_2(\mathbf{k}), \quad (2)$$

where $\delta_1(\mathbf{k})$ and D_{in} are the linear density and the linear growth factor evaluated at the initial redshift. The second-order term is given by

$$\delta_2(\mathbf{k}) = \sum_{\mathbf{p}} F_2(\mathbf{p}, \mathbf{k} - \mathbf{p}) \delta_1(\mathbf{p}) \delta_1(\mathbf{k} - \mathbf{p}), \quad (3)$$

with

$$F_2(\mathbf{p}, \mathbf{q}) = \frac{5}{7} + \frac{\mathbf{p} \cdot \mathbf{q}}{2} \left(\frac{1}{p^2} + \frac{1}{q^2} \right) + \frac{2}{7} \frac{(\mathbf{p} \cdot \mathbf{q})^2}{p^2 q^2}. \quad (4)$$

We sum up all the modes up to the Nyquist frequency (256^3 modes in total) in equation (3). Here, equation (4) includes the fastest growing mode. Bernardeau, Crocce & Scoccimarro (2008) recently present the correct formula of F_2 including the sub-leading growing mode.

Let us explicitly write the amplitude and the phase of a mode as

$$\delta(\mathbf{k}, z) = |\delta(\mathbf{k}, z)| \exp(i\phi(\mathbf{k}, z)), \quad (5)$$

Then the evolution of amplitude in each mode is

$$\frac{\hat{P}(k, z)/\hat{P}(k, z_{\text{in}})}{D(z)^2/D_{\text{in}}^2} = 1 + \frac{1}{N_k} \sum_{|\mathbf{k}|=k} 2\text{Re} [\delta_1(\mathbf{k}) \delta_2^*(\mathbf{k})] \times \frac{1}{\hat{P}(k, z_{\text{in}})} \frac{D(z)}{D_{\text{in}}}, \quad (6)$$

whereas the phase evolution is

$$\phi(\mathbf{k}, z) - \phi_{\text{in}}(\mathbf{k}) = \sin \phi_{\text{in}}(\mathbf{k}) \cos \phi_{\text{in}}(\mathbf{k}) \times \left(\frac{\text{Im} \delta_2(\mathbf{k})}{\text{Im} \delta_1(\mathbf{k})} - \frac{\text{Re} \delta_2(\mathbf{k})}{\text{Re} \delta_1(\mathbf{k})} \right) \frac{D(z)}{D_{\text{in}}}, \quad (7)$$

up to second order. The expressions in equations (6) and (7) are independent of the initial redshift for the late time ($D \gg D_{\text{in}}$), since $\delta_1 \propto D_{\text{in}}$ and $\delta_2 \propto P(k, z_{\text{in}}) \propto D_{\text{in}}^2$. We do not distinguish between δ and δ_1 at the initial redshift ($z_{\text{in}} = 30$), since δ_2 is much smaller than δ_1 at that time.² and provide more detail analysis.

It is clear from equation (4) that nonlinear mode-coupling occurs with particular sets of wavenumber vectors such that $\mathbf{p} + \mathbf{q} = \mathbf{k}$. From equation (4), we obtain

$$F_2(\mathbf{p}, \mathbf{k} - \mathbf{p}) \rightarrow \left(\frac{3}{14} - \frac{5}{7} \cos^2 \theta \right) \frac{k^2}{p^2}, \quad (8)$$

for $k \ll p$, and

$$F_2(\mathbf{p}, \mathbf{k} - \mathbf{p}) \rightarrow \frac{1}{2} \frac{k}{p} \cos \theta, \quad (9)$$

for $k \gg p$. Here θ is an angle between \mathbf{k} and \mathbf{p} . Hence the coupling to the mode of much smaller scale $p(\gg k)$ is negligibly weak, while the coupling to much larger scale $p(\ll k)$ is strong. In summary, most of the contribution to the second-order evolution of a mode comes from the modes of comparable scales or larger.³

For a Gaussian random field, the mode amplitudes are Rayleigh-distributed, and thus there is a finite probability that a mode has a very large or a very small amplitude with respect to the expected *mean* value. Some peculiar modes, which have very large or very small amplitudes compared to the mean, strongly affect the growth of other modes through the mode-coupling as described in the above.

In an ideal situation where there are infinite number of modes, the second term in equation (6) vanishes. In that case, the leading correction arises from the forth order of δ_1 . Then the resultant power spectrum with the one-loop correction is,

$$P_{1\text{loop}}(k, z) = \left(\frac{D(z)}{D_{\text{in}}} \right)^2 P_{11}(k) + \left(\frac{D(z)}{D_{\text{in}}} \right)^4 [P_{22}(k) + P_{13}(k)], \quad (10)$$

where $P_{11} = \langle |\delta_1|^2 \rangle$, $P_{22} = \langle |\delta_2|^2 \rangle$, $P_{13} = 2 \langle \text{Re}[\delta_1 \delta_3^*] \rangle$ (Makino, Sasaki & Suto 1992; Jain & Bertschinger 1994; Jeong & Komatsu 2006). We integrate from $k = 2\pi/L$ to the Nyquist frequency in the calculation of P_{22} and P_{13} .

² Nishimichi et al. (in preparation) distinguish δ from δ_1 at the initial epoch with the 2LPT initial condition (Crocce, Pueblas & Scoccimarro 2006)

³ Muecket et al. 1988 examined the growth of the small-scale perturbation on the background of the large-scale perturbation.

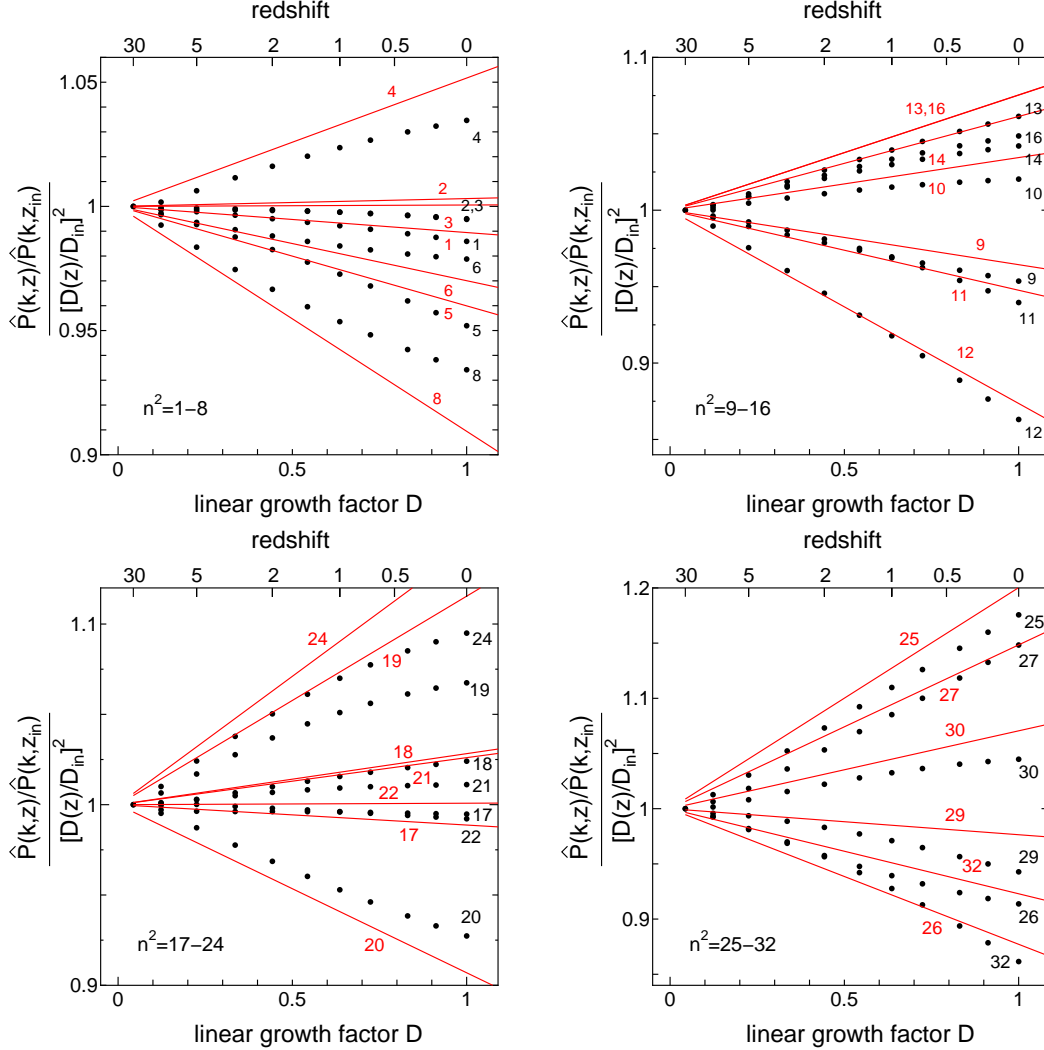


Figure 2. Evolution of the deviation of the power amplitude with respect to the linear theory prediction. The dots are the measurements from our simulation, and red solid lines are the model prediction using the second-order perturbation theory. The integers denote $n^2 = n_1^2 + n_2^2 + n_3^2$ of wavenumbers, and the figures show different range of n^2 , $n^2 = 1 - 8$ (upper left panel), $n^2 = 9 - 16$ (upper right panel), $n^2 = 17 - 24$ (lower left panel), and $n^2 = 25 - 32$ (lower right panel).

The dashed lines in Fig.1 are the one-loop power spectrum at each redshift. It suggests that the linear theory is applicable for $k < 0.07h/\text{Mpc}$ at $z = 0$. However, the finite mode coupling in the second term of equation (6) significantly changes the evolution of the power spectrum even in the linear regime.⁴

Fig.2 shows the evolution of the mean amplitude of modes with identical wavenumber n^2 in the range of 1 – 32. Here, $n^2 \simeq 30$ corresponds to the position of the first peak (see Fig.1). The four panels are for $n^2 = 1 - 8$ (upper left panel), $n^2 = 9 - 16$ (upper right panel), $n^2 = 17 - 24$ (lower left panel), and $n^2 = 25 - 32$ (lower right panel). The dots are the measurement from simulation outputs, and red solid lines are the theoretical prediction from the initial density fields at $z_{in} = 30$ in equation (6). The second-order perturbation theory reproduces the simulation results rather well.

The theory fits the data within 0.5% at $z = 2$ and 2% at $z = 0$ for larger scale ($n^2 = 1 - 8$), whereas within 1% at $z = 2$ and 10% at $z = 0$ for smaller scale ($n^2 = 25 - 32$). This is because the second order perturbation theory is applicable at large scales and/or at high redshift.

Fig.3 is the same as Fig.2, but for phase evolution. We plot the results only for modes with $n_1 \geq n_2 \geq n_3$, because the mean of the phase at k , $\sum \phi(\mathbf{k})$, is zero (since $\phi(\mathbf{k}) + \phi(-\mathbf{k}) = 0$). The phase shifts are typically ≈ 0.1 radian at $z = 0$. Perturbation theory well reproduces the results. Even if there are infinite modes, the right hand side of equation (7) still remains. The phase shift is not due to the finite box size effect.

Previously Ryden & Gramann (1991) and Gramann (1992) studied the evolution of amplitude and phase in each mode using two dimensional simulations. They also calculated second-order perturbation theory and found the deviation from the linear theory grows in proportional to the scale factor in the EdS model. Sugimotohara & Suto (1991),

⁴ Seto (1999) also investigated the finite mode effect on the one-loop correction terms, $P_{22} + P_{13}$, in equation (10).

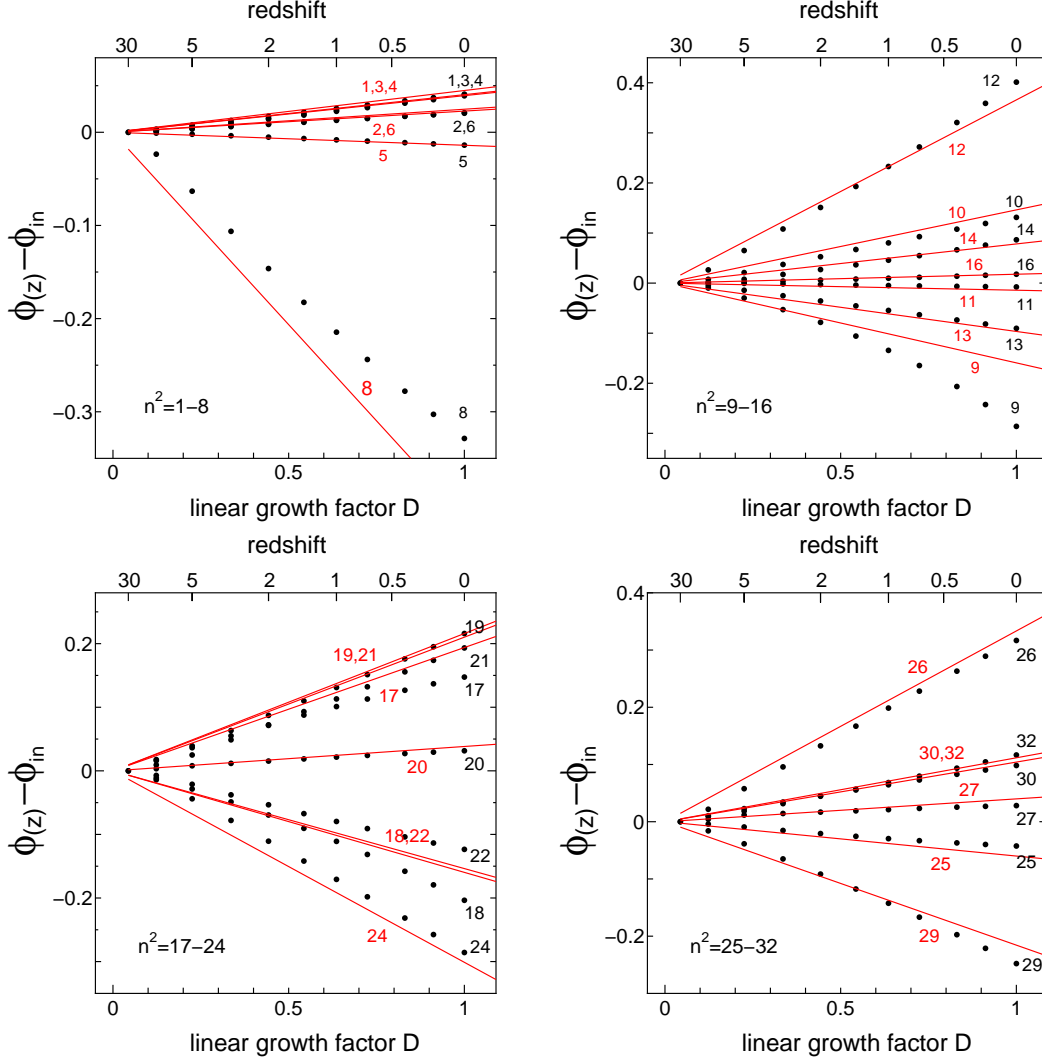


Figure 3. Same as Fig.2, but for phase evolution in units of radians. We plot the results only for modes with $n_1 \geq n_2 \geq n_3$.

Soda & Suto (1992) and Jain & Bertschinger (1998) also examined the nonlinear evolution in each mode. However they did not compare the theoretical prediction with the simulation results in detail. Their motivations were to understand the evolution of the density fluctuations in the nonlinear regime, whereas our interest here is in the growth of perturbations at the *linear* scale.

5 STATISTICAL ANALYSIS

The previous section considers second-order effects for a single realization. In this section we run 100 simulations to calculate dispersions of amplitude and phase deviations from linear theory. We prepare the 100 realizations for each of three box sizes of $L = 500h^{-1}\text{Mpc}$, $1h^{-1}\text{Gpc}$, and $2h^{-1}\text{Gpc}$, and $z_{\text{in}} = 30, 20$ and 10 , respectively.

Fig.4 shows the remaining amplitude dispersions from the linear theory prediction after correcting for the initial randomness at $z = 0$ for $L = 500h^{-1}\text{Mpc}$ (top), $1h^{-1}\text{Gpc}$ (middle), and $2h^{-1}\text{Gpc}$ (bottom). Since we already subtract the initial deviations due to the Gaussian distribution,

the residuals arise from the mode-coupling during the evolution. The grey dots with error bars are the means with 1σ scatters. By using a sufficiently large number of realizations, the means converge to the true values (solid line), and the magnitude of the dispersions is insensitive to the number of realizations. For $L = 500h^{-1}\text{Mpc}$, the dispersions are $\sim 10\%$ near the first peak, and $\sim 5\%$ even for a very large volume of $2h^{-1}\text{Gpc}$ on a side. The dashed lines show the theoretical prediction of the 1σ scatter, which is the rms (root-mean-square) of the second term in equation (6) :

$$\begin{aligned} \sigma_{\text{amp}}^2 &\equiv \left\langle \left(\frac{\hat{P}(k, z)/\hat{P}(k, z_{\text{in}})}{D(z)^2/D_{\text{in}}^2} - 1 \right)^2 \right\rangle \\ &= \frac{4P_{22}(k, z_{\text{in}})}{P_{11}(k, z_{\text{in}})} \frac{1}{\Delta N_k} \left(\frac{D(z)}{D_{\text{in}}} \right)^2. \end{aligned} \quad (11)$$

Here, ΔN_k is the number of modes in the bin, $\Delta N_k = 4\pi n^2 \Delta n$ with $n = (L/2\pi)k$. In this unbinned case, the number of modes is $\Delta N_k = kL\Delta n^2$ (with $\Delta n^2 = 1$). The dashed lines well reproduce the results.

Fig.4 also shows the results for the binned data of $\Delta k =$

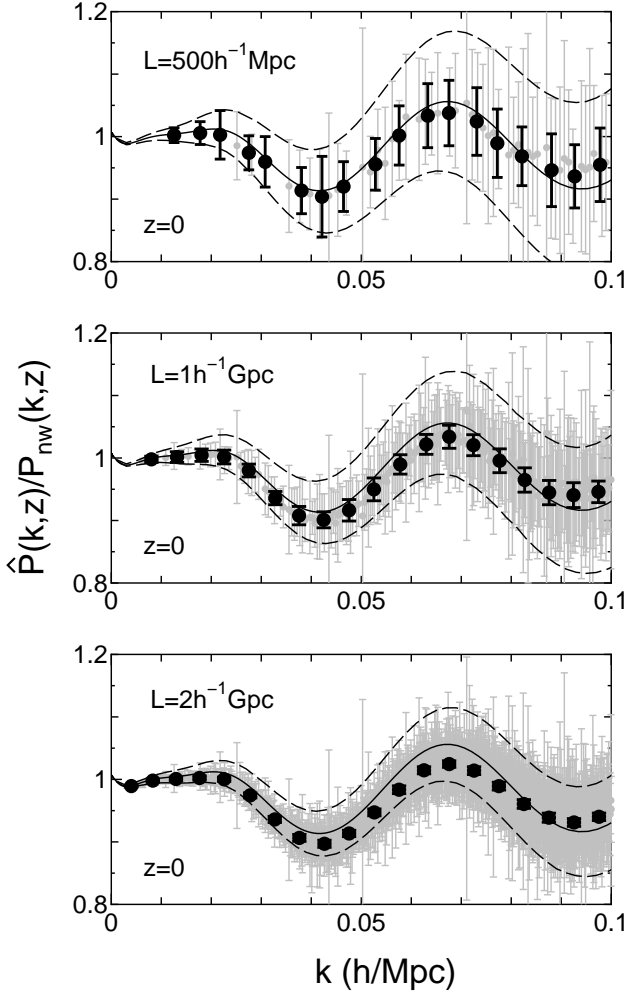


Figure 4. The amplitude dispersions of the 100 realizations at $z = 0$ for $L = 500h^{-1}$ Mpc (top), $1h^{-1}$ Gpc (middle), and $2h^{-1}$ Gpc (bottom). The grey dots with error bars are for the unbinned data, while the black big symbols are for the binned data of $\Delta k = 0.005h/\text{Mpc}$. The value of k for the binned data is the weighted mean of k with the number of wavenumbers in the bin. The dashed lines are the theoretical prediction.

$0.005h/\text{Mpc}$ by the black big symbols. In this case, we use the power spectrum defined as $\hat{P}(k) = (1/\Delta N_k) \sum |\delta(\mathbf{k})|^2$, summing up all the modes between $(k - \Delta k/2, k + \Delta k/2)$, instead of equation (1). Here, the number of modes in the bin is

$$\Delta N_k = (L^3 k^2)/(2\pi^2) \Delta k. \quad (12)$$

We calculate the means and error bars for the binned $\hat{P}(k)$.

Fig.5 shows the amplitude dispersions calculated from our simulation outputs for $\Delta k = 0.005h/\text{Mpc}$ (filled circle) and the theoretical prediction (solid line). From this figure with equations (11) and (12), we find that the dispersion is approximated as

$$\sigma_{\text{amp}}(z=0) \simeq 2\% \left(\frac{L}{1\text{Gpc}/h} \right)^{-3/2} \left(\frac{\Delta k}{0.005h/\text{Mpc}} \right)^{-1/2}, \quad (13)$$

at $k = 0.02 - 0.1h/\text{Mpc}$. The dispersion is proportional to $\Delta N_k^{-1/2} \propto L^{-3/2} \Delta k^{-1/2}$ from equation (12). Note that even

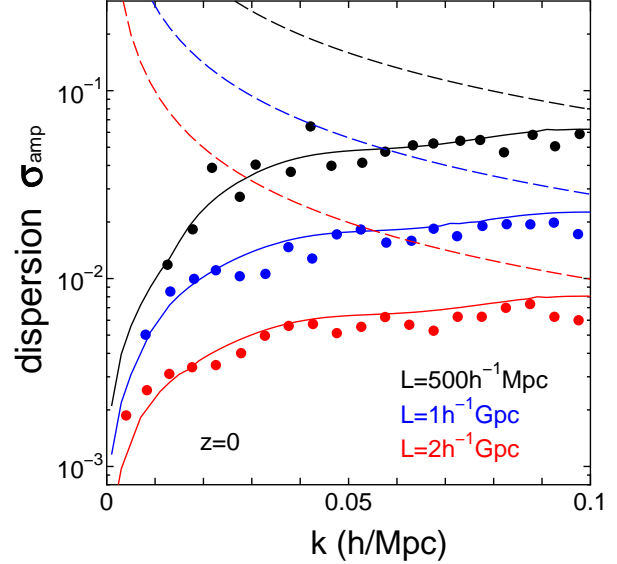


Figure 5. The amplitude dispersions calculated from our simulation outputs (filled circle \bullet) and the theoretical predictions (solid lines). We also show the dispersions due to the initial Gaussian distribution (dashed lines). The vertical dotted line is the position of the BAO first peak.

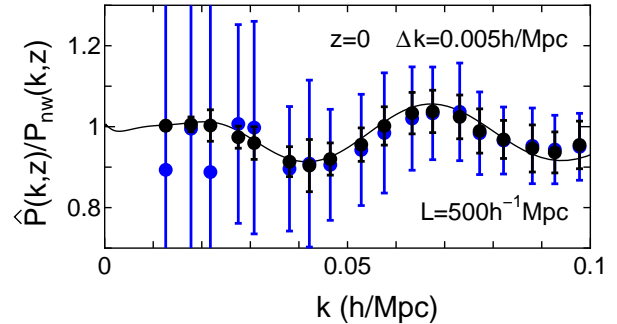


Figure 6. We compare two dispersions. Blue points with error bars show intrinsic scatter around the expected mean power spectrum for initial Gaussian random density fields. Black points show the dispersions owing to the finite nonlinear mode-coupling effect.

with a large simulation volume of $L \sim 1$ Gpc with k -binning, the dispersions still remain at the level of a few percent.

So far we have discussed the amplitude of deviations from linear theory. Here we also consider the intrinsic scatter of the initial Gaussian random realizations. In Fig.5 the dashed line is the dispersion for the initial distribution, which is given by $^5 (\Delta N_k/2)^{-1/2}$. Fig.5 shows that the dashed lines decrease as $\propto (\Delta N_k)^{-1/2} \propto k^{-1}$, while the solid lines increase because P_{22}/P_{11} increases (see equation [11]). These two dispersions are comparable at $k \simeq 0.1h/\text{Mpc}$ where $2P_{22}/P_{11} \simeq 1$ at $z = 0$. About a half of the dispersions near the position of the BAO first peak ($k \sim 0.07h/\text{Mpc}$) are attributed to the second-order effects. The result suggests that, at large scales, $k < 0.1h/\text{Mpc}$, the dispersions arise mainly from the initial Gaussian random distribution,

⁵ The number of modes ΔN_k is divided by 2 because the Fourier modes of $\delta(\mathbf{k})$ and $\delta(-\mathbf{k})$ are not independent.

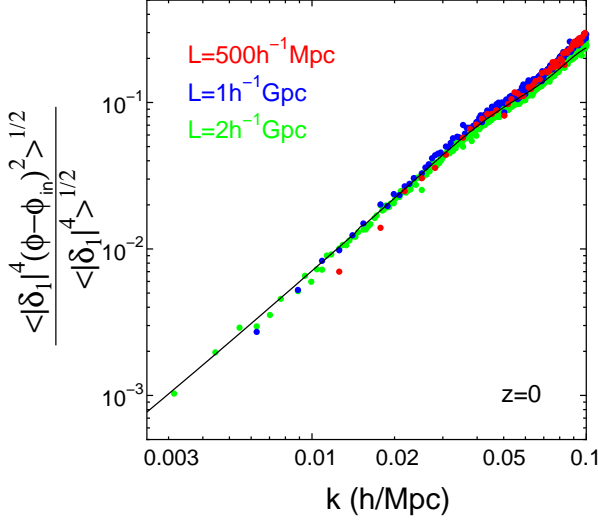


Figure 7. The phase dispersion of the 100 realizations. The solid line is the theoretical prediction.

while at smaller scale $k > 0.1h/\text{Mpc}$ they are from the mode-coupling (based on the second or higher order perturbation) during the evolution. In Fig.6 the blue symbols are the results for our 100 realizations. The black symbols are same as in the top panel of Fig.4 for $\Delta k = 0.005h/\text{Mpc}$. As expected, the initial random realizations have larger scatters around the mean expected power spectrum, especially at the largest scales.

We have also performed a similar analysis for the evolution of the mode phases (equation [7]). Fig.7 shows the phase dispersion calculated from our simulations (the dots). Here we set $-\pi \leq (\phi - \phi_{in}) \leq \pi$ and calculate $\langle |\delta_1|^4 (\phi - \phi_{in})^2 \rangle$ instead of $\langle (\phi - \phi_{in})^2 \rangle$. This is because $(\phi - \phi_1) \propto 1/\delta_1$ in Eq.(7) and its dispersion diverges at $\delta_1 = 0$. We obtain the phase dispersion from equation (7) as,⁶

$$\frac{\langle |\delta_1(\mathbf{k})|^4 [\phi(\mathbf{k}, z) - \phi_{in}(\mathbf{k})]^2 \rangle}{\langle |\delta_1(\mathbf{k})|^4 \rangle} = \frac{P_{22}(k, z_{in})}{6P_{11}(k, z_{in})} \left(\frac{D(z)}{D_{in}} \right)^2. \quad (14)$$

The solid lines are the theoretical prediction, which fit the simulation results well. The phase dispersion in equation (14), as well as the amplitude dispersion in equation (11), are independent of the initial redshift. In the non-linear limit of $k \rightarrow \infty$, the phases are distributed randomly, and the phase dispersion approaches to $\pi/\sqrt{3}$ rad (e.g. Ryden & Gramann 1991).

6 DISCUSSION AND CONCLUSIONS

In this paper, we critically examined how accurately cosmological N -body simulations describe the evolution of large-scale density distributions, particularly focusing on the linear and/or quasi-linear scales. For the power spectrum calculated from a single realization, we found that the growth of large-scale fluctuations significantly deviates from the linear theory prediction, and the enhanced or suppressed growth

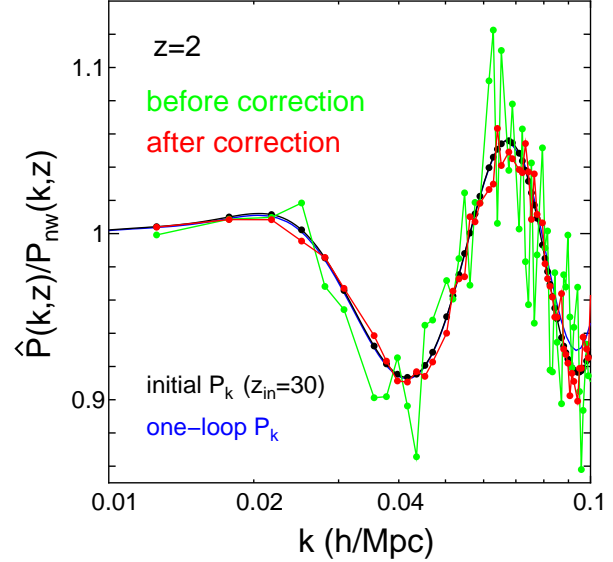


Figure 8. The power spectrum at $z = 2$. The green line is the simulation output. In the red line, we subtract the second-order perturbation contribution from the simulation output. The blue line is the one-loop power spectrum.

of perturbations produces an ugly noisy pattern in the matter power spectrum. This deviation is not due to the numerical errors in the N -body code, but due to the non-linear coupling between finite numbers of modes originating from the finite box size. To study the effect of the finite mode-coupling in detail, we developed perturbation theory and quantitatively estimated the finite-mode coupling to the power spectrum amplitude. Mode-by-mode analysis in three-dimensional Fourier space reveals that the finite mode-coupling from the second-order perturbation is sufficient to explain the deviation from linear theory prediction on large scales. The dispersion of the mode-coupling effects estimated from second-order perturbation scales as $\propto L^{-3/2} \Delta k^{-1/2}$, and this may surpass the intrinsic scatter of the initial Gaussian distribution. Since the finite mode-coupling does not vanish even for a large-volume simulation, it is of critical importance to correct it properly for high-precision studies of baryon acoustic oscillations.

We show that the perturbative approach is very helpful to quantify the significance of finite-mode coupling and this can be utilized as an efficient and powerful tool to correct the finite-mode coupling. As an example, in Fig. 8, we evaluate the power spectrum directly obtained from a single realization at $z = 2$, and subtract the finite-mode coupling using the second-order perturbation. Compared the result before subtraction with that after subtraction, the deviation from linear theory is dramatically reduced and the noisy structures are effectively wiped out. As a result, even the single realization data of N -body simulation faithfully reproduces the linear theory prediction on large scales.

Although the present paper mainly concerns with the second-order perturbation theory, higher-order perturbations are also important for the relevant scales of the measurement of baryon acoustic oscillations, where the acoustic signature tends to be erased by the effect of non-linear clustering (e.g. McDonald 2007; Crocce & Scoccimarro 2007;

⁶ Jain & Bertschinger (1996) previously derived equation (14) with an approximation for the long-wave mode coupling.

Matsubara 2007b; Taruya & Hiramatsu 2008). The height of the first peak is found to be reduced about 2% (J. Wang, A. Szalay et al. in preparation). Thus, the inclusion of the higher-order terms may be important for the estimation of the finite-mode coupling, which would be helpful to further reduce the noisy structures on small scales.

We note that the variance of the growth of matter power spectrum with respect to the linear theory prediction, $\langle[(\hat{P}/\hat{P}_{\text{lin}})/(D/D_{\text{lin}})^2 - 1]^2\rangle$, which we have studied, is different from the variance of the power spectrum itself, $\langle(\hat{P} - P)^2\rangle$. It remains unclear if the numerical effects studied here are important in evaluating covariance matrices (e.g., Scoccimarro, Zaldarriaga & Hui 1999; Meiksin & White 1999; Neyrinck & Szapudi 2007). In future work, we will study nonlinear and numerical effects in the power spectrum covariance using a large set of simulations and analytic models.

ACKNOWLEDGMENTS

We thank Jie Wang, Erik Reese, and Simon White for useful comments and discussions. We also thank the anonymous referee for careful reading and useful suggestions. This work is supported in part by Grant-in-Aid for Scientific Research on Priority Areas No. 467 “Probing the Dark Energy through an Extremely Wide and Deep Survey with Subaru Telescope”, by the Mitsubishi Foundation, and by Japan Society for Promotion of Science (JSPS) Core-to-Core Program “International Research Network for Dark Energy”, and by Grant-in-Aids for Scientific Research (Nos. 18740132, 18540277, 18654047). T. N., A. S. and K. Y. are supported by Grants-in-Aid for Japan Society for the Promotion of Science Fellows.

REFERENCES

- Angulo R.E., Baugh C.M., Frenk C.S., & Lacey C.G., 2008, *MNRAS*, 383, 755
- Bagla J.S. & Prasad J., 2006, *MNRAS*, 370, 993
- Bernardeau F., Colombi S., Gaztanaga E., & Scoccimarro R., 2002 *Physics Reports*, 367, 1
- Bernardeau F., Crocce M., & Scoccimarro R., 2008, *arXiv:0806.2334*
- Cole S., et al., 2005, *MNRAS*, 362, 505
- Crocce M., Pueblas S. & Scoccimarro R., 2006, *MNRAS*, 373, 369
- Crocce M. & Scoccimarro R., 2008, *PRD*, 77, 023533
- Eisenstein D.J., Hu W. & Tegmark M., 1998, *ApJ*, 504, L57
- Eisenstein D.J. & Hu W., 1998, *ApJ*, 496, 605
- Eisenstein D.J. et al., 2005, *ApJ*, 633, 560
- Gramann M., 1992, *ApJ*, 401, 19
- Guzik J., Bernstein G. & Smith R.E., 2007, *MNRAS*, 375, 1329
- Huff E., et al., 2007, *Astroparticle Physics*, 26, 351
- Jain B. & Bertschinger E., 1994, *ApJ*, 431, 495
- Jain B. & Bertschinger E., 1996, *ApJ*, 456, 43
- Jain B. & Bertschinger E., 1998, *ApJ*, 509, 517
- Jeong D. & Komatsu E., 2006, *ApJ*, 651, 619
- Lewis A., Challinor A. & Lasenby A., 2000, *ApJ*, 538, 473
- Makino N., Sasaki M. & Suto, Y., 1992, *PRD*, 46, 585
- Matsubara T., 2004, *ApJ*, 615, 573
- Matsubara T., 2007a, *ApJS*, 170, 1
- Matsubara T., 2008, *PRD*, 77, 063530
- Meiksin T. & White M., 1999, *MNRAS*, 308, 1179
- McDonald P., 2007, *PRD*, 75, 043514
- Muecket J.P., et al., 1998, *A&A*, 203, 211
- Neyrinck M.C. & Szapudi I., 2008, *MNRAS*, 384, 1221
- Nishimichi T., et al., 2007, *PASJ*, 59, 1049
- Okumura T., et al., 2008, *ApJ*, 676, 889
- Percival W.J., et al., 2007, *MNRAS*, 381, 1053
- Ryden B.S. & Gramann M., 1991, *ApJL*, 383, 33
- Scoccimarro R., Zaldarriaga M. & Hui L., 1999, *ApJ*, 527, 1
- Seo H.J. & Eisenstein D.J., 2003, *ApJ*, 598, 720
- Seo H.J. & Eisenstein D.J., 2005, *ApJ*, 633, 575
- Seto N., 1999, *ApJ*, 523, 24
- Smith R.E., Scoccimarro R. & Sheth R.K., 2007, *PRD*, 75, 3512
- Smith R.E., Scoccimarro R. & Sheth R.K., 2008, *PRD*, 77, 3525
- Soda J. & Suto Y., 1992, *ApJ*, 396, 379
- Spergel D.N., et al., 2007, *ApJ*, 170, 377
- Springel V., Yoshida N. & White S.D.M., 2001, *New Astronomy*, 6, 79
- Springel V., 2005, *MNRAS*, 364, 1105
- Springel V., et al., 2005, *Nature*, 435, 629
- Suginohara T. & Suto Y., 1991, *ApJ*, 371, 470
- Taruya A. & Hiramatsu T., 2008, *ApJ*, 674, 617

This paper has been typeset from a \LaTeX file prepared by the author.